Article

Chinese Science Bulletin

Optics

September 2010 Vol.55 No.26: 2930–2936
doi: 10.1007/s11434-010-4048-9

Near-field coupling and SERS effects of palladium nanoparticle dimers

RUAN FangXiong[1], ZHANG ShunPing[2], LI ZhiPeng[2], YANG ZhiLin[1,2*], WU DeYin[3], REN Bin[3] & XU HongXing[2]

[1] *Department of Physics, Xiamen University, Xiamen 361005, China;*
[2] *Institute of Physics, Chinese Academy of Sciences, Beijing 100190, China;*
[3] *Department of Chemistry, Xiamen University, Xiamen 361005, China*

Received February 11, 2010; accepted April 21, 2010

The linear optical properties and the surface-enhanced Raman scattering (SERS) effect of spherical palladium nanoparticle dimers are analyzed theoretically using generalized Mie theory. The calculation results demonstrate that the near-field coupling effect greatly influences the absorption, scattering and extinction spectra of nanoparticle dimers. The surface plasmon resonance wavelength red-shifts dramatically as the separation between nanoparticles decreases. Because of the near-field coupling between nanoparticles and the size effect, the maximum SERS enhancement factor at the 'hot spot' between palladium nanoparticle dimers is as high as 10^7–10^8, while the averaged SERS enhancement factor over the entire nanoparticle surface is in the range of 10^5–10^6. The deviation between the position of the peak in the extinction spectrum and the wavelength for maximum surface-averaged enhancement for the Pd nanoparticle dimers indicates that localized surface plasmon resonance has different influences on the far and near fields. These theoretical results may help to reveal the relationship between the far and near fields, as well as understand the mechanism of electromagnetic enhancement in the surface-enhanced scattering of transition metals.

surface-enhanced Raman scattering, near-field coupling, Mie scattering, transition metals, palladium

Citation: Ruan F X, Zhang S P, Li Z P, et al. Near-field coupling and SERS effects of palladium nanoparticle dimers. Chinese Sci Bull, 2010, 55: 2930–2936, doi: 10.1007/s11434-010-4048-9

Metal nanostructures have a large number of potential applications in biological and chemical sensors, surface-enhanced Raman scattering (SERS), photothermal therapy and optical communication because of their unique optical and electrical properties [1–5]. Tian's group successfully extended SERS from noble metals to various pure transition metals, including Rh, Pd, Ni, Pt and Ru, which is of both fundamental and practical importance [6–14]. They revealed that for transition metals, the SERS enhancement factor is as high as 10^4 under optimum experimental conditions. It is of great importance to study theoretically the optical properties of transition metal nanoparticles and aggregates to understand the underlying physical mechanism behind transition metal SERS [15–17].

Single molecule SERS studies have confirmed that the large enhancement is strongly dependent on the effect of near-field electromagnetic (EM) coupling between nanoparticles. The maximum electromagnetic enhancement factor of individual metal nanoparticles rarely exceeds 3 or 4 orders of magnitude even under the optimal conditions for localized surface plasmon resonance (LSPR). Xu et al. proved both theoretically and experimentally that the 'hot spot' in the nanogap is crucial for single molecule SERS [18,19]. It was found that a huge local EM enhancement factor can be obtained at the junction between a dimer of metal nanoparticles that are separated by several nanometers when an appropriate excitation frequency and polarization are used. Because of the near-field EM coupling effect,

*Corresponding author (email: zlyang@xmu.edu.cn)

the SERS factor at the 'hot spot' is larger than 10^{12} [20,21]. In this work, taking this interparticle coupling effect into consideration, we focus our theoretical studies on nanoparticle dimers rather than isolated nanoparticles. This will be critical to quantitatively understand the optical properties, particularly the SERS activity, of real SERS-active systems.

The methods proposed for solving the EM scattering problems of metal nanoparticles have been divided into numerical and analytical approaches. The numerical methods are comprised of *T*-matrix methods [22,23], finite element methods (FEM) [24], discrete dipole approximation (DDA) [25,26] and finite differential-time domain (FDTD) [27–31]. The Mie theory is the main analytical approach. Although numerical calculation methods are capable of simulating the optical properties of nanoparticles with arbitrary shapes effectively, Mie theory is a more rigorous and powerful tool for spherical nanoparticles or nanoparticle arrays. Mie theory is a model analysis method that depends on an exact solution to Maxwell's equations, and it is often regarded as the standard for testing the reliability and accuracy of other numerical calculation methods because of its accuracy and efficiency. Conventional Mie theory, which was first introduced by the Danish physicist Lorenz, was developed as an analytical method to explain the optical properties of gold colloids observed by Mie in 1908 [32]. Since then it has been widely used to calculate EM scattering properties of spherical particles with various sizes [33,34]. In recent years, the use of Mie theory has been extended from single spherical particles to multisphere systems, and the simulations of the far-field spectra and the near-field distribution of spherical particles with strong coupling have been achieved [35–38]. In this work, the optical properties and near-field enhancement of dimers of Pd nanospheres were simulated using generalized Mie theory. The dependence of the extinction spectrum and SERS enhancement on the separation of the two nanoparticles, particle size, excitation frequency and polarization were quantitatively investigated. Both the maximum local SERS enhancement factor at the 'hot spot' and the surface-averaged SERS enhancement factor were calculated and are discussed in detail.

1 Calculation method and model

According to [35], the incident and scattered EM fields can be expanded in infinite series of vector spherical harmonics (VSHs) $\boldsymbol{M}_{mn}^{j}$ and $\boldsymbol{N}_{mn}^{j}$ on the basis of conventional Mie theory [32], while $\boldsymbol{N}_{mn}^{j}=\frac{1}{k}\nabla\times\boldsymbol{M}_{mn}^{j}$ and $\boldsymbol{M}_{mn}^{j}=\frac{1}{k}\nabla\times\boldsymbol{N}_{mn}^{j}$ [39]. For simplicity, VSH is denoted as $\left|nmjp\right\rangle$, with p=1 for $\boldsymbol{M}_{mn}^{j}$ and p=2 for $\boldsymbol{N}_{mn}^{j}$, respectively. An incident field can be expanded in an infinite series of VSHs to

$$\left|i,E\right\rangle=\sum_{n=1}^{\infty}\sum_{m=-n}^{n}\left(CM_{mn}\left|nm11\right\rangle+CN_{mn}\left|nm12\right\rangle\right), \quad (1)$$

$$\left|i,H\right\rangle=\frac{k}{i\omega\mu}\sum_{n=1}^{\infty}\sum_{m=-n}^{n}\left(CM_{mn}\left|nm12\right\rangle+CN_{mn}\left|nm11\right\rangle\right). \quad (2)$$

For a plane wave, the expansion coefficients can be described as

$$CM_{mn}=\frac{2\pi i^{n}}{n(n+1)}\Big\{-(iE_x-E_y)\sqrt{(n+m+1)(n-m)}Y^{*}_{n,m+1}(\hat{\boldsymbol{k}})$$

$$-(iE_x+E_y)\sqrt{(n-m+1)(n+m)}Y^{*}_{n,m-1}(\hat{\boldsymbol{k}})+2imE_zY^{*}_{n,m}(\hat{\boldsymbol{k}})\Big\}, \quad (3)$$

$$CN_{mn}=\frac{2\pi i^{n}}{n(n+1)}\Bigg\{n\sqrt{\frac{(n+m+1)(n+m+2)}{(2n+1)(2n+3)}}(iE_x-E_y)Y^{*}_{n+1,m+1}(\hat{\boldsymbol{k}})$$

$$-n\sqrt{\frac{(n-m+1)(n-m+2)}{(2n+1)(2n+3)}}(iE_x+E_y)Y^{*}_{n+1,m-1}(\hat{\boldsymbol{k}})$$

$$-(n+1)\sqrt{\frac{(n-m-1)(n-m)}{(2n-1)(2n+1)}}(-iE_x+E_y)Y^{*}_{n-1,m+1}(\hat{\boldsymbol{k}})$$

$$-(n+1)\sqrt{\frac{(n+m-1)(n+m)}{(2n-1)(2n+1)}}(iE_x+E_y)Y^{*}_{n-1,m-1}(\hat{\boldsymbol{k}})$$

$$+\begin{bmatrix}2in\sqrt{\dfrac{(n+m+1)(n-m+1)}{(2n+1)(2n+3)}}Y^{*}_{n+1,m}(\hat{\boldsymbol{k}})\\ -2i(n+1)\sqrt{\dfrac{(n+m)(n-m)}{(2n-1)(2n+1)}}Y^{*}_{n-1,m}(\hat{\boldsymbol{k}})\end{bmatrix}E_z\Bigg\}, \quad (4)$$

where E_x, E_y and E_z are the three orthogonal components of the incident electric field $\boldsymbol{E}$, $\hat{\boldsymbol{k}}$ is the direction of the incident wave and $Y_{n,m}(\hat{\boldsymbol{k}})$ are spherical harmonics for $\hat{\boldsymbol{k}}$.

On the basis of the order-of-scattering method described in [35], in a spherical dimer system, the scattered field from each sphere is the sum of all of the orders of scattering, and can be represented as

$$\boldsymbol{E}_1^{s}=\sum_{n=1}^{\infty}\left(S_1+S_2M_{21}S_1\right)(M_{12}S_2M_{21}S_1)^{n-1}$$

$$=\frac{S_1+S_2M_{21}S_1}{1-M_{12}S_2M_{21}S_1}, \quad (5)$$

$$\boldsymbol{E}_2^{s}=\sum_{n=1}^{\infty}\left(S_2+S_1M_{12}S_2\right)(M_{21}S_1M_{12}S_2)^{n-1}$$

$$=\frac{S_2+S_1M_{12}S_2}{1-M_{21}S_1M_{12}S_2}, \quad (6)$$

where S_1 and S_2 represent the scattered field by spheres 1 and 2, respectively. M_{12} and M_{21} denote the coordinate transfers of the two spheres from each other, while n is the

order of scattering. Thus, the total scattered field is the sum of the scattered fields from the two spheres:

$$\boldsymbol{E}^s = \boldsymbol{E}_1^s + \boldsymbol{E}_2^s = \frac{S_1 + S_2 M_{21} S_1}{1 - M_{12} S_2 M_{21} S} + \frac{S_2 + S_1 M_{12} S_2}{1 - M_{21} S_1 M_{12} S_2}. \quad (7)$$

Meanwhile, the normal modes for the scattered wave are changed to the first-order spherical Hankel forms: $|nm31\rangle$ and $|nm32\rangle$ by exchanging the spherical Bessel functions j_n to the spherical Hankel functions $h_n^{(1)} = j_n + iy_n$. To calculate the scattering field for a spherical dimer system expediently, we defined the following matrixes:

$$C_m = \left[CM_{m1}\ CM_{m2}\ \cdots\ CM_{mN}\ CN_{m1}\ CN_{m2}\ \cdots\ CN_{mN}\right],$$

$$W_m^{E,h} = \left[|1m31\rangle\ |2m31\rangle\ \cdots\ |Nm31\rangle\ |1m32\rangle\ |2m32\rangle\ \cdots\ |Nm32\rangle\right]^{\mathrm{T}},$$

$$W_m^{H,h} = \left[|1m32\rangle\ |2m32\rangle\ \cdots\ |Nm32\rangle\ |1m31\rangle\ |2m31\rangle\ \cdots\ |Nm31\rangle\right]^{\mathrm{T}},$$

$$S_1 = \left[{}^1b_1\ \ {}^1b_2\ \ \cdots\ \ {}^1b_N\ \ {}^1a_1\ \ \cdots\ \ {}^1a_N\right]^{\mathrm{D}},$$

$$S_2 = \left[{}^2b_1\ \ {}^2b_2\ \ \cdots\ \ {}^2b_N\ \ {}^2a_1\ \ \cdots\ \ {}^2a_N\right]^{\mathrm{D}},$$

$$M_{12}^m = \begin{bmatrix} A_{m1}^{m1} & A_{m2}^{m1} & \cdots & A_{mN}^{m1} & B_{m1}^{m1} & B_{m2}^{m1} & \cdots & B_{mN}^{m1} \\ A_{m1}^{m2} & A_{m2}^{m2} & \cdots & \cdots & B_{m1}^{m2} & B_{m2}^{m2} & \cdots & \cdots \\ \cdots & \cdots & \cdots & \cdots & \cdots & \cdots & \cdots & \cdots \\ A_{m1}^{mN} & \cdots & \cdots & A_{mN}^{mN} & B_{m1}^{mN} & \cdots & \cdots & B_{mN}^{mN} \\ B_{m1}^{m1} & B_{m2}^{m1} & \cdots & B_{mN}^{m1} & A_{m1}^{m1} & A_{m2}^{m1} & \cdots & A_{mL}^{m1} \\ B_{m1}^{m2} & B_{m2}^{m2} & \cdots & \cdots & A_{m1}^{m2} & A_{m2}^{m2} & \cdots & \cdots \\ \cdots & \cdots & \cdots & \cdots & \cdots & \cdots & \cdots & \cdots \\ B_{m1}^{mN} & \cdots & \cdots & B_{mN}^{mN} & A_{m1}^{mN} & \cdots & \cdots & A_{mN}^{mN} \end{bmatrix},$$

where D represents a diagonal matrix and N is the number of multipole. In Cartesian coordinates, the scattered EM field vector matrixes can be mathematically deduced as

$$\boldsymbol{E}^s = \sum_{m=-N}^{N} C_m \frac{\sqrt{S_1} + S_2 M_{21}^m \sqrt{S_1}}{1 - \sqrt{S_1} M_{12}^m S_2 M_{21}^m \sqrt{S_1}} \sqrt{S_1} \left({}^1W_m^{E,h}\right)$$

$$+\mathrm{e}^{i\boldsymbol{kd}} \sum C_m \frac{\sqrt{S_2} + S_1 M_{12}^m \sqrt{S_2}}{1 - \sqrt{S_2} M_{21}^m S_1 M_{12}^m \sqrt{S_2}} \sqrt{S_2} \left({}^2W_m^{E,h}\right), \quad (8)$$

$$\boldsymbol{H}^s = \frac{k}{i\omega\mu} \sum_{m=-N}^{N} C_m \frac{\sqrt{S_1} + S_2 M_{21}^m \sqrt{S_1}}{1 - \sqrt{S_1} M_{12}^m S_2 M_{21}^m \sqrt{S_1}} \sqrt{S_1} \left({}^1W_m^{H,h}\right)$$

$$+\mathrm{e}^{i\boldsymbol{kd}} \sum C_m \frac{\sqrt{S_2} + S_1 M_{12}^m \sqrt{S_2}}{1 - \sqrt{S_2} M_{21}^m S_1 M_{12}^m \sqrt{S_2}} \sqrt{S_2} \left({}^2W_m^{H,h}\right), \quad (9)$$

where $\boldsymbol{d}$ is the vector from the center of sphere 1 to the center of sphere 2.

Then, according to the definition of total far field cross sections [32], if a spherical surface is chosen to enclose the objects, the extinction and scattering cross sections can be described as

$$Q_{ext} = -\frac{1}{k^2} \mathrm{Re}\left(\sum_{n=1}^{\infty} \sum_{m=-n}^{n} \frac{1}{n(n+1)} \times \left(\langle s|nm31\rangle \langle nm11|i\rangle + \langle s|nm32\rangle \langle nm12|i\rangle \right) \right), \quad (10)$$

$$Q_s = \frac{1}{k^2} \mathrm{Re}\left(\sum_{n=1}^{\infty} \sum_{m=-n}^{n} \frac{1}{n(n+1)} \times \left(\langle s|nm31\rangle \langle nm31|s\rangle + \langle s|nm32\rangle \langle nm32|s\rangle \right) \right), \quad (11)$$

where $\langle s|nm31\rangle$, $\langle s|nm32\rangle$ and $\langle nm11|i\rangle$, $\langle nm12|i\rangle$ represent the scattering and incident coefficients, respectively.

The theoretical model used in this work consists of two identical Pd nanospheres with the particle diameter D and a separation distance d, as schematically illustrated in Figure 1. In the calculation, the surrounding medium was assumed to have a refractive index of 1.0 that corresponds to air, and a plane wave of 1 V/m with an amplitude that is incident along the y-axis direction, with the polarization parallel to the interparticle axis (z-axis). The center cross-section, passing through the midpoint of the gap between the nanoparticles, is perpendicular to the z-axis. The dielectric function of palladium was taken from [40], and all of the calculations are based on generalized Mie theory.

2 Results and discussion

2.1 Near-field coupling effect

It is known that the interparticle surface plasmon resonance (SPR) coupling effect plays the key role in increasing the local field enhancement factor of nanoparticle dimers illuminated by a laser. If the excitation polarization is perpen-

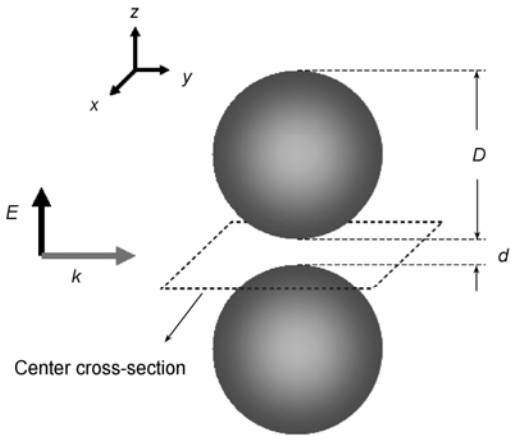

Figure 1 Schematic diagram of the Pd nanosphere dimers illuminated by a plane wave.

dicular to the interparticle axis connecting the centers of the two nanospheres (hereafter named the perpendicular-polarized excitation mode), the interaction between spherical metal nanoparticle dimers and incident light will be very weak, resulting in a small SERS enhancement. In this case, the SERS of the dimer is simply the sum of the two isolated nanoparticles, and the SERS enhancement factor of the nanosphere dimer remains in the same order as a single nanoparticle. However, if the excitation polarization is parallel to the interparticle axis (known hereafter as the parallel-polarized excitation mode), the SPR coupling effect will be strong enough to form a 'hot spot' at the junction between the nanosphere dimers at a particular excitation frequency. Thus, it is crucial for transition metals, which have lower SERS activity than noble metals in the visible light region, to enhance the SERS signal of adsorbed molecules using the strong EM enhancement at the 'hot spot'.

First, Mie calculations were performed to quantitatively investigate the impact of near-field coupling on the extinction spectra of Pd nanosphere dimers with a particle diameter D = 100 nm with the parallel-polarized excitation mode (Figure 2(a)). The figure shows that for a single Pd nanosphere with D = 100 nm, a peak appears at 335 nm in the ultraviolet region of the extinction spectrum. For a nanosphere dimer, near-field coupling of the particles leads to pronounced red shifts in the plasmon resonance wavelength. The extinction peaks exhibit increasing width and intensity as the particle separation decreases. When the gap distance (d) between the nanoparticles is smaller than about 30 nm, the extinction peak shifts into the visible light region. The extinction peaks, which correspond to local SPR, are found at 401, 454, 497, 530 and 566 nm when d is 30, 10, 4, 2 and 1 nm, respectively. The SPR peak intensity is the greatest when the separation distance reduces to 2–1 nm. Further calculations showed that the interparticle coupling is negligible and the extinction spectrum of Pd nanosphere dimers is almost the same as that of a single nanosphere when d>>D.

Besides the significant influence on the extinction spectrum, the interparticle coupling effect also leads to a dramatic local EM field enhancement on the nanoparticle surface because of localized SPR, which is the essential EM enhancement mechanism of SERS. Here, the SERS enhancement factor of Pd nanosphere dimers was quantitatively studied. To obtain the theoretical results which could be compared directly with experimental data, the surface-averaged SERS enhancement factors of probe molecules adsorbed at different surface positions on the nanoparticle dimers (assuming a monolayer of molecules were uniformly adsorbed on the surface) was calculated; the results are shown in Figure 2(b). In the calculation, the enhanced Raman scattering intensity from a probe molecule at any given position is considered approximately proportional to the fourth power of the electric field enhancement at the position of the molecule and any Raman shift is ignored. For a single Pd nanosphere with a diameter of 100 nm, the maximum surface-averaged SERS enhancement is less than two orders of magnitude under laser excitation with an optimal frequency (442 nm). For Pd dimers, the calculation results showed that the excitation wavelength that gives the maximum surface-averaged enhancement factor of SERS red shifts gradually with decreasing d. For d of 30, 10, 4, 2 and 1 nm, the peak positions for the maximum SERS enhancement are located at 537, 565, 584, 601 and 651 nm, respectively. It can also be seen that the maximum surface-averaged enhancement factor increases continuously as the near-field coupling effect increases accompanying the decreasing d. When d is less than 10 nm, the maximum SERS enhancement factor increases in an approximately exponential way as d decreases. At d of 10 and 4 nm, the maximum SERS enhancement factors are 10^3 and 10^4, respectively. When d reduces to 1 nm, the maximum SERS factor dramatically increases to 5×10^5. Because the maximum SERS enhancement factor of Pd nanosphere dimers with d = 1 nm is about three orders of magnitude higher than that of a single nanosphere, it is expected that the SERS activity is very low for individual nanoparticles in SERS experiments.

By comparing the results in Figure 2(a) and (b), we found that, although the peak positions of extinction spectrum

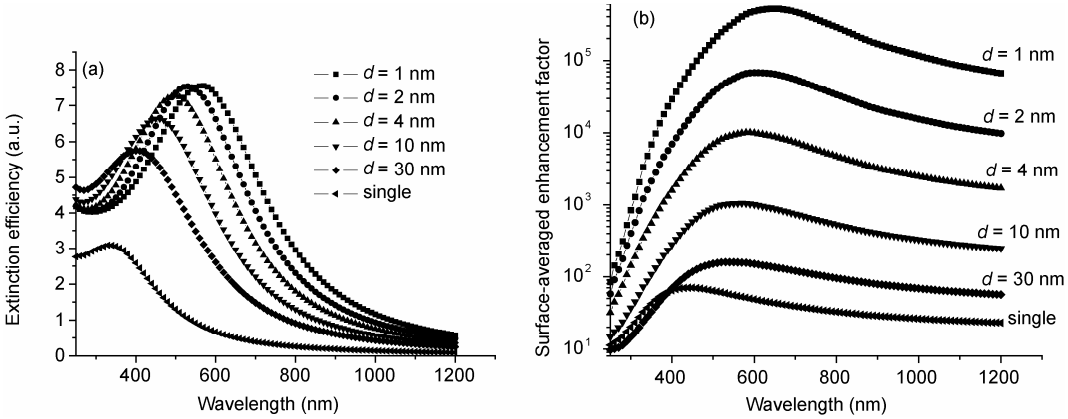

Figure 2 Incident wavelength dependent spectra of a single Pd nanosphere and Pd nanosphere dimers with D = 100 nm and various d. (a) Extinction efficiency; (b) surface-averaged SERS enhancement factor.

and the wavelength for the maximum surface-averaged enhancement both red-shift gradually with decreasing d, the peak positions of the two spectra are different at a fixed separation distance of Pd dimers. The 80–130 nm deviation in the peak position between the two spectra for the same dimer reflects the different impacts of SPR on the far field (extinction spectrum) and the near field (SERS). The reasons for this deviation may be explained as follows. First, the extinction efficiency, which exhibits the characteristics of multipole radiation, is proportional to the polarizations of various multipoles, and higher order multipoles usually give a small contribution to the far field. However, for the near field, both the dipoles and higher order multipoles critically influence its electric field intensity. The interparticle SPR coupling effect has a great impact on the high order multipoles for the near-field, even playing a dominant role at times. Second, the near-field enhancement mainly originates from the scattering effect of nanoparticles, while the far-field extinction is composed of both absorption and scattering. In addition to the SPR effect, the interband transition also contributes to the absorption spectrum, which leads to a blue-shift of the absorption spectrum compared with the scattering spectrum. Therefore, the peak position of LSPR shown in the far-field UV-Vis spectrum is not always at the optimal excitation wavelength for SERS, and the latter shows a small red-shift from the former. It is of great importance that this discrepancy is noted for the experimental design and study of SERS.

The dependence of the extinction efficiency and SERS enhancement factor on the excitation wavelength of the Pd nanosphere dimers with D = 100 nm and d = 1 nm was further calculated to study the different influences of LSPR on the far and near fields. The results are shown in Figure 3. The two solid lines in the figure correspond to the extinction efficiency spectrum and surface averaged SERS enhancement spectrum respectively, and the discrete points represent the maximum SERS enhancement obtained at the 'hot spot' of a Pd dimer as the wavelength is varied.

The figure shows that the normalized curves of the extinction efficiency and the surface averaged enhancement factor reach their maximum at 556 and 651 nm, respectively. The curves for the maximum enhancement factor at the 'hot spot' and the surface-averaged enhancement factor almost overlap. Note that the three curves in the figure are normalized. The maximum SERS enhancement at the 'hot spot' is two orders of magnitude larger than that of the maximum surface-averaged enhancement. The surface-averaged enhancement curve shows a red shift of about 85 nm compared with the extinction spectrum, which suggests that the maximum SERS factor may not be achieved when the Pd dimer is excited at the extinction peak wavelength (the SPR excitation frequency). The maximum SERS enhancement factor at the 'hot spot' is at exactly the same wavelength as the maximum surface-averaged enhancement factor for the Pd dimer. This strongly indicates that the SERS signal of aggregated nanoparticles mainly results from those molecules located at the 'hot spot'. In other words, the SERS activity of Pd dimers is mainly dependent on the near field coupling effect in the gap between the two nanoparticles known as the 'hot spot'.

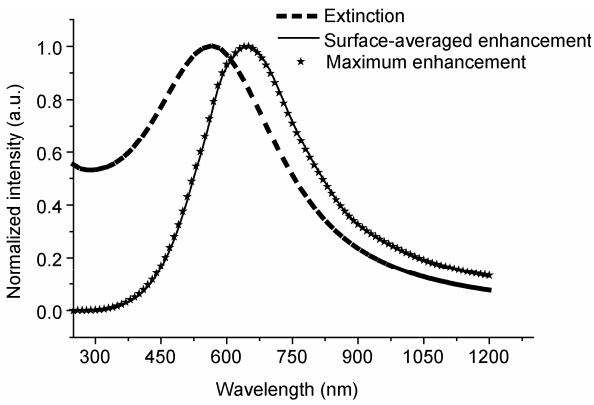

Figure 3 Incident wavelength dependent spectra of a Pd nanosphere dimer with D = 100 nm and d = 1 nm. The dashed line, solid line and discrete points correspond to the extinction efficiency, surface-averaged enhancement and maximum E-field enhancement factor, respectively.

To quantitatively obtain the SERS enhancement factors at different surface regions of Pd nanosphere dimers, we calculated and visualized the near-field distributions of Pd nanosphere dimers with D = 100 and d = 1 nm under 651 nm laser illumination using Mie theory. In this calculation, the incident electric vector $\boldsymbol{E}$ was polarized along the interparticle axis connecting the centers of the two spheres (Figure 4). From Figure 4(a), we can see clearly that the local electric field concentrates in a very small region (the so-called 'hot spot') in the gap between the dimers; the electric field in other regions decreases rapidly with increasing distance from the junction. For Pd dimers, the peak value of E^2 at the 'hot spot' is as high as about 10^4 because of the interparticle near-field coupling effect, which means the SERS enhancement factor is approximately 8 orders of magnitude if the Raman shift effect is neglected. Compared with a single particle, the emergence of a 'hot spot' with a huge EM enhancement factor for nanoparticle dimers explains why the SERS activity of individual metal nanoparticles is always much lower than that of aggregated nanoparticles.

The optical intensity (E^2) contours at the 'center cross-section' plane of the Pd dimers are shown in Figure 4(b) to highlight the detailed E-field distribution at the 'hot spot'. From this figure, it can be seen that the enhanced electric fields are confined within a small region (several nanometers in diameter) in the middle of the 'center cross-section' plane. The maximum local electric field at the 'hot spot' is 9105 times more than that of the incident field, corresponding to a SERS enhancement factor of 8×10^7 for molecules adsorbed at the 'hot spot'. The SERS enhancement factor decays almost exponentially as the distance from the centre of the 'hot spot' increases. This calculation result shows that the maximum SERS EM enhancement factor at the 'hot spot'

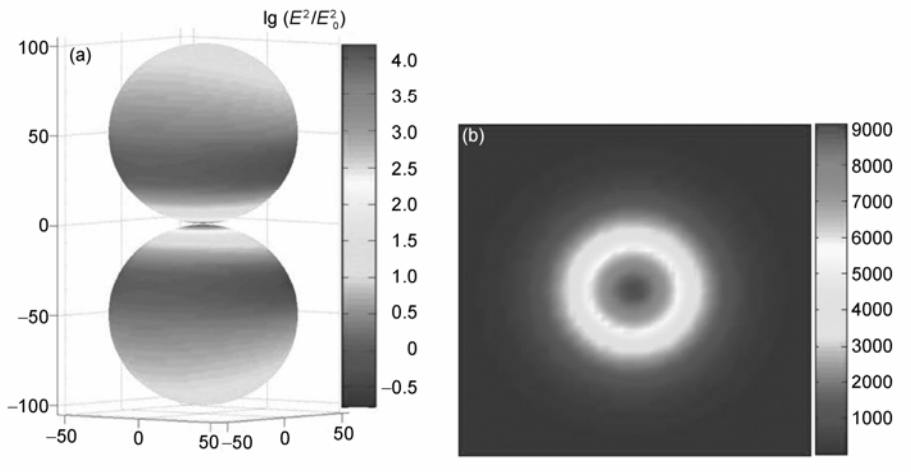

Figure 4 Theoretical calculations of the near-field optical intensity (E^2) contours above the surface of a Pd nanosphere dimer with D = 100 nm and d = 1 nm, under incident illumination at a wavelength of 651 nm. (a) The enveloping surface at a distance of 0.01 nm from the dimer surface; (b) the "center cross-section" plane of the dimer.

of Pd nanosphere dimers is close to 8 orders of magnitude.

2.2 Particle size effect

The above discussions are based on a fixed Pd nanosphere size of 100 nm. In fact, the optical properties of nanoparticles (e.g. the intensity and position of plasmon resonance peaks) are also critically dependent on the size of nanoparticles because of the retardation of the EM field across metal clusters [41,42]. The quantitative influence of particle size on the near-field coupling of Pd nanosphere dimers under the parallel-polarized excitation mode was evaluated using Mie calculations. Figure 5 shows the dependence of the extinction efficiency and surface-averaged enhancement factor on the excitation wavelength for Pd nanosphere dimers with various sizes at a fixed d = 1 nm. As shown in Figure 5(a), the extinction peaks of LSPR are located at 257, 381, 475, 566 and 657 nm corresponding to D = 40, 60, 80, 100 and 120 nm, respectively. This result indicates that the SPR peak red-shifts gradually as the particle size increases. Figure 5(b) shows the surface-averaged enhancement factor as a function of the particle diameter. The surface averaged enhancement peaks appear at 379, 452, 530, 647 and 732 nm, corresponding to D = 40, 60, 80, 100 and 120 nm, respectively.

At a fixed separation distance, the wavelength for the maximum surface-averaged enhancement factor of Pd nanosphere dimers red-shifts gradually and the SERS enhancement factor increases monotonically with increasing particle size. The maximum SERS enhancement factor increases from about 2.5×10^4 to 5×10^5 as the size of the Pd nanosphere varies from D = 40 nm to D = 100 nm. However, the peak value for SERS enhancement remains in a narrow region of 10^5–10^6 when the particle size is above 100 nm.

3 Conclusions

The near-field coupling effect and the SERS effect of Pd nanosphere dimers were quantitatively studied using generalized Mie theory. The SPR wavelength red-shifts dramatically as the separation distance between the nanoparticles decreases, while the LSPR peak intensity increases gradu-

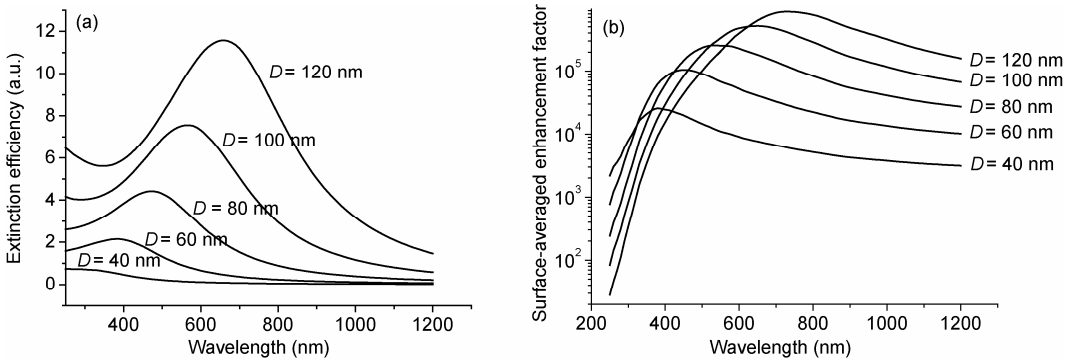

Figure 5 Incident wavelength dependent spectra of Pd nanosphere dimer with d = 1 nm and various D from 40 to 120 nm. (a) The extinction efficiency; (b) the surface-averaged enhancement factor.

ally. For Pd nanosphere dimers, the maximum SERS enhancement factor at the 'hot spot' is as high as 10^7–10^8, while the surface-averaged SERS enhancement factor is in the range of 10^5–10^6 under optimum conditions for the parallel-polarized excitation mode. There is deviation between the peak positions of the extinction spectrum and the wavelength for the maximum SERS enhancement in the Pd nanosphere system, which indicates that SPR has a different impact on the far field and near field. The nanoparticle size also influences the coupling effect, and the dimers containing larger particles usually show higher SERS activity. The theoretical results in this work may be helpful for further understanding the SERS enhancement mechanism, as well as for designing and optimizing SERS experiments with transition metals for practical use.

The authors wish to thank Professor Tian ZhongQun of Xiamen University for helpful discussion and valuable suggestions. This work was supported by the National Natural Science Foundation of China (20703032), National Basic Research Program of China (2009CB930703) and Natural Science Foundation of Fujian Province of China (E0710028).

1 Sonnichsen C, Alivisatos A P. Gold nanorods as novel nonbleaching plasmon-based orientation sensors for polarized single-particle microscopy. Nano Lett, 2005, 5: 301–304
2 Tian Z Q, Ren B, Li J F, et al. Expanding generality of surface-enhanced Raman spectroscopy with borrowing SERS activity strategy. Chem Commum, 2007, 34: 3514–3534
3 Huang X, El-Sayed I H, Qian W, et al. Cancer cell imaging and photothermal therapy in the near-infrared region by using gold nanorods. J Am Chem Soc, 2006, 128: 2115–2120
4 Ferry V E, Sweatlock L A, Pacifici D, et al. Plasmonic nanostructure design for efficient light coupling into solar cells. Nano Lett, 2008, 8: 4391–4397
5 Sukharev M, Seideman T. Phase and polarization control as a route to plasmonic nanodevices. Nano Lett, 2006, 6: 715–719
6 Tian Z Q, Ren B, Mao B W. Extending surface Raman spectroscopy to transition metal surfaces for practical applications 1. Vibrational properties of thiocyanate and carbon monoxide adsorbed on electrochemically activated platinum surfaces. J Phys Chem B, 1997, 101: 1338–1346
7 Ren B, Lin X F, Yang Z L, et al. Surface-enhanced Raman scattering in the ultraviolet spectral region: UV-SERS on rhodium and ruthenium electrodes. J Am Chem Soc, 2003, 125: 9598–9599
8 Wu D Y, Li J F, Ren B, et al. Electrochemical surface-enhanced Raman spectroscopy of nanostructures. Chem Soc Rev, 2008, 37: 1025–1041
9 Li J F, Yang Z L, Ren B, et al. Surface-enhanced Raman spectroscopy using gold-core platinum-shell nanoparticle film electrodes: Toward a versatile vibrational strategy for electrochemical interfaces. Langmuir, 2006, 22: 10372–10379
10 Fan F R, Liu D Y, Wu Y F, et al. Epitaxial growth of heterogeneous metal nanocrystals: From gold nano-octahedra to palladium and silver nanocubes. J Am Chem Soc, 2008, 130: 6949–6951
11 Tian Z Q, Ren B. Adsorption and reaction at electrochemical interfaces as probed by surface-enhanced Raman spectroscopy. Annu Rev Phys Chem, 2004, 55: 197–299
12 Liu Z, Yang Z L, Cui L, et al. Electrochemically roughened palladium electrodes for surface-enhanced Raman spectroscopy: Methodology, mechanism and application. J Phys Chem C, 2007, 111: 1770–1775
13 Cui L, Wang A, Wu D Y, et al. Shaping and shelling Pt and Pd nanoparticles for ultraviolet laser excited surface-enhanced Raman scattering. J Phys Chem C, 2008, 112: 17618–17624
14 Ren B, Liu G K, Lian X B, et al. Raman spectroscopy on transition metals. Anal Bioanal Chem, 2007, 388: 29–45
15 Yang Z L, Wu D Y, Yao J L, et al. SERS mechanism of nickel electrode. Chinese Sci Bull, 2002, 47: 1983–1986
16 Xiong Y, McLellan J M, Chen J, et al. Kinetically controlled synthesis of triangular and hexagonal nanoplates of palladium and their SPR/SERS properties. J Am Chem Soc, 2005, 127: 17118–17127
17 Yang Z L, Li Y, Li Z P, et al. Surface enhanced Raman scattering of pyridine adsorbed on Au@Pd core/shell nanoparticles. J Chem Phys, 2009, 130: 234705
18 Xu H X, Bjerneld E J, Kall M, et al. Spectroscopy of single hemoglobin molecules by surface enhanced Raman scattering. Phys Rev Lett, 1999, 83: 4357–4360
19 Xu H X, Aizpurua J, Kall M, et al. Electromagnetic contributions to single-molecule sensitivity in surface-enhanced Raman scattering. Phys Rev E, 2000, 62: 4318–4324
20 Moskovits M, Tay L L, Yang J, et al. SERS and the single molecule. Topics Appl Phys, 2002, 82: 215–227
21 Kneipp K, Kneipp H, Bohr H G. Single-molecule SERS spectroscopy. Topics Appl Phys, 2006, 103: 261–278
22 Peterson B, Strom S. *T* matrix for electromagnetic scattering from an arbitrary number of scatterers and representations of E(3). Phys Rev D, 1973, 8: 3361–3677
23 Mackowski D W, Mishchenko M I. Calculation of the *T* matrix and the scattering matrix for ensembles of spheres. J Opt Soc Am A, 1996, 13: 2266–2278
24 Brown R J C, Wang J, Milton M J T. Electromagnetic modeling of Raman enhancement from nanoscale structures as means to predict the efficacy of SERS substrates. J Nanomater, 2007, 1: 12086
25 Purcell E M, Pennypacker C R. Scattering and absorption of light by nanospherical dielectric grains. Astrophys J, 1973, 186: 705–714
26 Flatau P J, Fuller K A, Mackowski D W. Scattering by two spheres in contact: Comparisons between discrete-dipole approximation and modal analysis. Appl Opt, 1993, 32: 3302–3305
27 Yang Z L, Aizpurua J, Xu H X. Electromagnetic field enhancement in TERS configurations. J Raman Spectrosc, 2009, 40: 1343–1348
28 Taflove A. Computational Electrodynamics: The Finite-Difference Time-Domain Method. Boston, MA: Artech House, 1995
29 Novotny L, Bian R X, Xie X S. Theory of nanometric optical tweezers. Phys Rev Lett, 1997, 79: 645–648
30 Videen G, Sun W, Fu Q. Light scattering from irregular tetrahedral aggregates. Opt Commum, 1998, 156: 5–9
31 Ozbay E. Plasmonics: Merging photonics and electronics at nanoscale dimensions. Science, 2006, 331: 189–193
32 Mie G. Beitrage zur optik truber medien seziell kolloidaler matallosungen. Ann Phys, 1908, 25: 377–455
33 Xu H X, Kall M. Surface-plasmon-enhanced optical forces in silver nanoaggregates. Phys Rev Lett, 2002, 89: 246802
34 Comberg U, Wriedt T. Comparison of scattering calculations for aggregated particles based on different models. J Quant Spectrosc Radiat Transfer, 1999, 63: 149–162
35 Xu H X. A new method by extending Mie theory to calculate local field in outside/inside of aggregates of arbitrary spheres. Phys Lett A, 2003, 312: 411–419
36 Xu H X. Calculation of the near field of aggregates of arbitrary spheres. J Opt Soc Am A, 2004, 21: 804–809
37 Li Z P, Xu H X. Electromagnetic energy flow near metal nanoparticles-II: Algorithms for the calculation of the light scattering of multi-spheres and photon energy transport via linear chains of Ag nanoparticles. J Quant Spectrosc Radiat Transfer, 2007, 103: 394–401
38 Fuller K A. Optical resonances and two-sphere systems. Appl Opt, 1991, 30: 4716–4731
39 Stratton J A. Electromagnetic Theory. New York: McGraw-Hill, 1941
40 Johnson P B, Christy R W. Optical constants of transition metals: Ti, V, Cr, Mn, Fe, Co, Ni, and Pd. Phys Rev B, 1974, 9: 5056–5070
41 Mock J J, Barbic M, Smith D R, et al. Shape effects in plasmon resonance of individual colloidal silver nanoparticles. J Chem Phys, 2002, 116: 6755–6759
42 Grady N K, Halas N J, Nordlander P. Influence of dielectric function properties on the optical response of plasmon resonant metallic nanoparticles. Chem Phys Lett, 2004, 399: 167–171